American Society of Mechanical Engineers

ASME Accepted Manuscript Repository

Institutional Repository Cover Sheet

Cranfield Collection of E-Research - CERES

ASME Paper Title: Application of spectral method for vibration-induced high-cycle fatigue evaluation of an HP turbine blade

Authors: Iroizan Ubulom

ASME Journal Title: Journal of Engineering for Gas Turbines and Power

Volume/Issue: Volume 143, Issue 6 Date of Publication (VOR* Online): 11 November 2020

ASME Digital Collection URL: https://asmedigitalcollection.asme.org/gasturbinespower/article/doi/10.1115/1.4049099/1090628/Application-of-Spectral-Method-for

DOI: https://doi.org/10.1115/1.4049099

*VOR (version of record)

Journal of Engineering for Gas Turbines and Power. Received August 26, 2020; Accepted manuscript posted November 11, 2020. doi:10.1115/1.4049099
Copyright (c) 2020 by ASME
Journal of Engineering for Gas Turbines and Power, Volume 143, Issue 6, June 2021, Article number GTP-20-1395

Application of Spectral Method for Vibration-Induced High-Cycle Fatigue Evaluation of an HP Turbine Blade

Iroizan Ubulom

Center for Propulsion Engineering, School of Aerospace, Transport and Manufacturing (SATM), Cranfield University, Bedford, MK430AL, United Kingdom

ABSTRACT

A method of fluid-structure interaction coupling is implemented for a forced-response, vibration-induced fatigue life estimation of a high-pressure turbine blade. Two simulations approaches; a two-way (fully-coupled) and one-way (uncoupled) methods are implemented to investigate the influence of fluid-solid coupling on a turbine blade structural response. The fatigue analysis is performed using the frequency domain spectral moments estimated from the response power spectral density of the two simulation cases. The method is demonstrated in relation to the time-domain method of the rainflow cycle counting method with mean stress correction. Correspondingly, the mean stress and multiaxiality effects are also accounted for in the frequency domain spectral approach. In the mean stress case, a multiplication coefficient is derived based on the Morrow equation, while the case of multiaxiality is based on a criterion which reduces the triaxial stress state to an equivalent uniaxial stress using the critical plane assumption. The analyses show that while the vibration-induced stress histories of both simulation approaches are stationary, they violate the assumption of normality of the frequency domain approaches. The stress history profile of both processes can be described as platykurtic with the distributions having less mass near its mean and in the tail region, as compared to a Gaussian distribution with an equal standard deviation. The fully-coupled method is right leaning with positive skewness while the uncoupled approach is left leaning with negative skewness. The directional orientation of the principal axes was also analyzed based on the Euler angle estimation. Although noticeable differences were found in the peak distribution of the normal stresses for both methods, the predicted Euler angle orientations were consistent in both cases, depicting a similar orientation of the critical plane during a crack initiation process. Finally, the fatigue life estimation was shown to be conservative in the fully-coupled solution approach.

***(Keywords**: turbine blade, high-cycle fatigue, Dirlik damage method, spectral moments, and probability density functions)*

1) INTRODUCTION

The structural issues often encountered in the design and operability of the turbine blades offer a unique problem case. The load pattern and stress distributions are due to a complex interplay of aerodynamic, thermal and structural loads. Such problems lie in the domain of a coupled fluid-structure interaction study. Fluid-Structure Interaction (FSI) is a multidisciplinary solution approach which considers the interplay/interaction between the two fields of fluid and structural response. This formulation of the interaction between the two-fields have been aided by the separate development of the finite element and computational fluid dynamics codes, previously allowing them to be treated separately without any form of multi-physics interaction. While numerous studies have been performed highlighting the application of fluid-structure interactions to turbine blade problems [1], very little information exist on the influence of this higher-fidelity and computationally expensive approach on the solution procedure, nonetheless, in relation to fatigue life estimation. The current work implements two levels of fluid-structure interaction couplings to investigate its impact on the spectral fatigue life of a high-pressure gas turbine blade.

Of interest to this current study is the influence of fluid-solid coupling on the High-Cycle Fatigue (HCF) loading condition of a high-pressure gas turbine blade. For the HCF mode, the problem is mostly attributed to the unsteady aerodynamic influence which is able to excite the blade in one of its vibration modes, Fleeter et al. [2]. At a failure condition, the excitation frequency coincides with the blade natural frequency, thereby resulting in peak amplitudes stresses with significant life consumption. This is, therefore, of a multidisciplinary nature given that the aerodynamic and mechanical loads act concurrently on the blades. For a downstream component such as a turbine blade located after the combustor and nozzle-guide vanes, any resulting flow unsteadiness, for instance due to shock-waves in the passage or severe distortion of the combustor pattern factor, can result in high amplitude vibrational forces. In the current study, the influence of the unsteady airflow from upstream stator blades is modelled in addition to the large mean stresses arising from the centrifugal forces of the rotating wheel. In the high-cycle failure mode, the resulting blade vibration and induced strains are mostly elastic in nature but occurring

Published by The American Society of Mechanical Engineers. This is the Author Accepted Manuscript issued with: Creative Commons Attribution License (CC BY). The final published version is available online at DOI:10.1115/1.4049099. Please refer to any applicable publisher terms of use.

at very high-frequencies in a short span. This complex interplay requires an accurate life prediction approach which is essential to avoid any likelihood of an overly expensive designed model, or underutilizing the remaining useful life [3].

Conventionally, the unsteady flow problem is modelled as a forced response loading case where the turbine blade is subjected to random loadings from the unsteady aerodynamic sources. Thus, in a classical forced-response analysis of a stator-rotor configuration, the response of the model to the random loading is viewed in lieu of the power spectral density of the corresponding stresses. In assessing the severity of the impact of such damages, time-domain methods are widely used which often require the prior estimation of the full local time histories. Following to this, the fatigue damage is determined based on the cycle counting method of the rainflow approach. The effect of cumulative damage arising from prior loading history is then analyzed using the Palmgren-Miner damage summation method which is carried out via a linear superposition of the independent damage states. The relevant stress history is analyzed for the cycle damage induced per unit time. However, in considering that a large number of sample time history data is required to provide sufficient information on the induced cycles, this invariably implies a tedious and computationally intensive fatigue analysis approach for the time-domain methods. As noted by Carpinteri et al. [4], the damage evaluation using the time-domain approach can also be susceptible to errors resulting from the uncertainty present in the cycle counting algorithm of the rainflow approach. Thus, the development of a newer method is necessary which can provide a quick assessment of the structural integrity of the blades, with relatively cheaper and less computationally intensive efforts.

To this end, it has been shown that enormous time savings can be achieved if such analyses are performed using the frequency domain approach. As noted by [5], the limitations of the probabilistic analysis of time-domain can be avoided by using the frequency domain approach which allows the multiaxial stress state to be represented using the power spectral density parameter. This eliminates the scatter inherent in the process as the fatigue life can be predicted based on the estimated spectral moments of the Power Spectral Density (PSD). The spectral moments which are bandwidth parameters and are obtained from the variance and autocorrelation matrix of the induced stress. This study therefore assesses the applicability of this alternative frequency domain, spectral fatigue damage methods for structural integrity assessment of an aerospace turbine blade under a random vibration, forced-response high-cycle fatigue loading**.**

The method is implemented for the fatigue damage estimation of a high-pressure turbine blade subjected to a forced-response loading with the stress state predicted using the two approaches of a two-way and a one-way fluid-structure interaction coupling. The two-way and one-way solution approaches are hereafter described as fully-coupled and uncoupled solution approaches. The influence of fluid-solid coupling is investigated through a spectral evaluation of the power spectral density parameters of the two simulation approaches. In the fully-coupled case, the solutions of the fluid and finite element models are obtained concurrently with information transfer implemented through a fluid-solid interface. For the uncoupled simulation case, the independent computations of the fluid and solid-side problems are performed with the unsteady pressure fields from the fluid-side model used as a boundary condition in the finite element model. In both approaches, the issue of non-stationarity and the presence of mean stresses are addressed. The frequency domain fatigue analysis is thereafter compared with solutions obtained from the time-domain approach of rainflow cycle counting. Such comparisons will be useful in highlighting the relevance and applicability of the spectral domain method for the fatigue damage estimation of a gas turbine blade

2) FLUID-STRUCTURE INTERACTION MODELLING

In the current work, the forced-response problem of the turbine blade stage is modelled using a fluid-structure interaction solver. The unsteady aerodynamics of the stator-rotor interaction case is predicted using a compressible flow solver, CFX, which is coupled to an ANSYS finite element solver in a staggered solution approach. The conditions of compatibility and energy conservation at the fluid-solid interface is ensured through multiple iterations of the solution variables per solution time step. Two levels of fluid-solid coupling, referred to as: fully-coupled and uncoupled solution approaches are implemented to investigate the influence of the multiphysics interaction on the spectral fatigue properties of the turbine blade. In the fully-coupled method, the fatigue life input stress history is obtained through a concurrent solution of the blade structural equation of motion and that of the compressible 3D fluid flow case. The information transfer between the two domains is implemented via a common interface with regular updates of the solution variables via a feedback loop that couples the two solvers per solution timestep. Approximately, 10-coupling iterations were allowed at each timestep to ensure the conservation of variables and compatibility conditions at the interface. This resulted in a tight coupling procedure which allows for an automatic inclusion of the aerodynamic damping term, which is often separately estimated in the unilateral data transfer approach of the uncoupled method. However, the difficulty associated with this method

is the longer computation time that is required to obtain a fully converged solution, given that several iterations are often required to ensure a tight convergence per solution timestep. The analysis procedure for the fully-coupled process is as represented in Figure 1.The process involves several sub-cycling steps within a particular timestep in a means to ensure that kinematic and conservation conditions at the fluid-solid interface are met. The fatigue analysis is incorporated in the post-processing stage after the solution convergence is obtained.

At the fluid-solid interface, the kinematic condition assumes the continuity of the velocity field at the interface. Thus, in a viscous flow case, this is represented in the form:

$$T_r(U^s)_{|\Gamma} = T_r(U^f)_{|\Gamma,} \quad 1$$

And for an inviscid flow case;

$$T_r(U^s.n)_{|\Gamma} = T_r(U^f.n)_{|\Gamma,} \quad 2$$

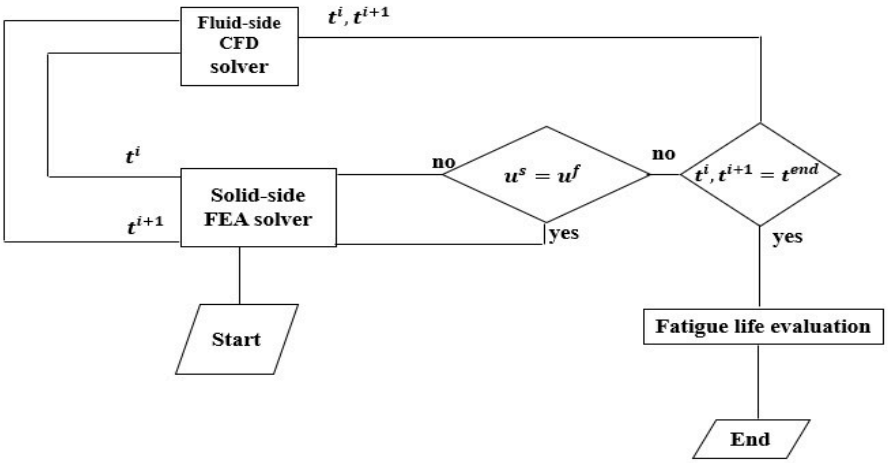

Figure 1 SOLUTION PROCEDURE FOR FULLY-COUPLED APPROACH

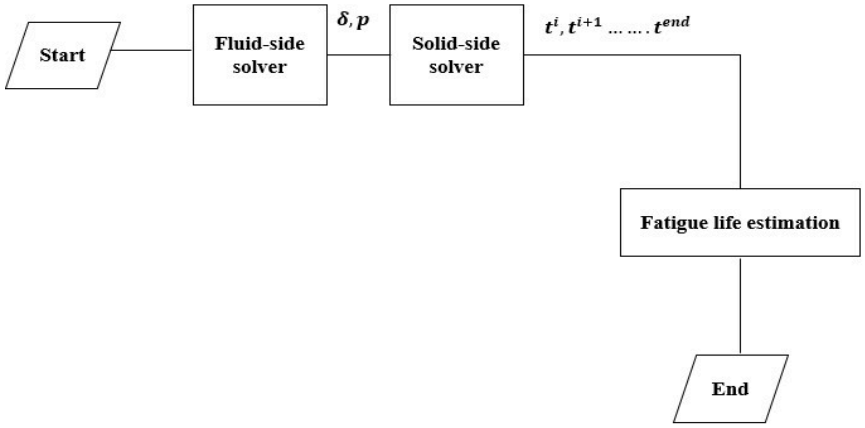

Figure 2 SOLUION PROCEDURE FOR UNCOUPLED PROCEDURE

where "T_r" is the trace operation signifying the restriction applied to the interface, and "U^f" is the surface variable at the fluid interface. "U^s" is the corresponding variable on the solid-domain interface, and n is the unit normal vector.

Similarly, in maintaining the energy balance at the interface boundary, the related dynamic conditions are maintained through the relation:

$$\underline{d_f} = \underline{d_s} \quad 3$$

$$n_f.\underline{\tau_f} = -n_s.\underline{\tau_s} \quad 4$$

where d_f, d_s are the fluid-side and solid-side displacement conditions, respectively. τ_i is the stress tensor, and n_f, n_s are the unit normal vectors pointing outwards respectively from the fluid and solid domains. The benefit of the implemented method is that the separate gauss integration points can be chosen independently for the fluid

and solid stiffness matrices. The method ensures energy conservation in the fluid-solid interface, Γ, through its computation of surface traction (moments and forces) parameters.

In the second method of uncoupled analysis, the unsteady aerodynamic analysis is performed independently, and the estimated pressure fields are transferred as boundary conditions to the solid finite element model. As shown in Figure 2 the method is performed without any feedback loop between the two fields as the two solutions are obtained separately. The argument in support of this method is its simplicity in implementation as most commercially available solvers have this capability. The method is readily implemented with reduced computational time, given that no sub-cycling within each timestep is required to ensure conservation and compatibility condition as required of the two-way method. The uncoupled method allows the use of separate solvers without the need in formulating an interface/coupling algorithm to couple the independent codes, [6]. As a first step in this method, an initial 3D flow field analysis is performed to establish the unsteady forcing which is utilized as boundary condition in the finite element code to predict the unsteady stresses and subsequent fatigue life estimation. Due to the unilateral transfer of the computed fluid pressures to the solid-finite element code, it is necessary to ensure minimal error during the coupling process. For instance, [7] reported a potential loss in accuracy and magnitude of the estimated load response if this is not implemented accurately. In this current work, this error was minimized through the projection of the unsteady forces using a Cartesian coordinate interpolation, thus maintaining the exact interface coordinates in both domains. Given that the solutions of the fluid and solid-side equations are considered as an independent computational framework, the treatment of the interface condition is explicitly handled, without any need for a feedback loop to connect the two domains. The only need for an interface in this case, is therefore to ensure the accurate transfer of the surface pressure loads to the finite element nodal elements. The Cartesian interpolation approach uses a wetted area-averaging method to interpolate the load variables. The Transfer Error (TE) which indicates the accuracy of the method was determined using the correlation:

$$TE = {f_p - s_p}/{f_p} * 100 \quad (5)$$

where f_p, s_p are the respective fluid-side (computed) and solid-side (interpolated) pressure values. In this case, the transfer error was quantitatively estimated at less than 0.1%.

As shown in Figure 2, a key parameter in the accurate implementation of this approach is the estimation of the aerodynamic damping term δ. The total damping sources on turbomachinery components are mainly from three sources: mechanical, aerodynamic and material. While the mechanical sources are introduced through instances such as frictional contacts and the viscoelastic layer damping, the material damping sources are mainly from hysteretic sources due to cyclic deformation [8] The third sources, which is of interest in this approach is the aerodynamic damping sources. It is mainly due to the unsteady work done by the surface pressures acting on the blade in a vibratory manner. In the absence of friction dampers, the aerodynamic damping source is considered as the dominant factor in the estimation of the vibration response, while the mechanical damping term is obtained from the material properties which were specified as temperature dependent in the solver.

With regards to the aerodynamic damping term, the log-decrement component, δ, can be estimated from the relation:

$$\delta = {1}/{n_i} \, ln\left(\frac{x_i}{x_{i+1}}\right) \quad (6)$$

where x_i, x_{i+1} represent the peak and successive peak values of the signal and n_i is the total number of peaks in the stress signals. From the logarithmic decrement term, the total aerodynamic damping ratio can be determined from;

$$\zeta_{aero} = \frac{\delta}{\sqrt{4\pi + \delta^2}} \quad (7)$$

$$\zeta_{Total} = \zeta_{aero} + \zeta_{mech} \quad (8)$$

Both the aerodynamic (ζ_{aero}) and mechanical damping (ζ_{mech}) terms were modelled based on the non-dimensional decay constants, ζ_{Total}. The blade response in the flow case is due mainly to the influence of hourglass viscosity and that from the unsteady pressure. A similar method for estimating the damping of a turbomachinery blade undergoing multiple vibration modes in a time domain simulation of a fluid-structure interaction analysis was presented in Gottfried and Fleeter [9]. In using the above method, an estimated value of

the aerodynamic damping was obtained from the pressure field history on the blade surface. In the current case, an estimated value of 0.6% was obtained which is in the range of typical values expected for a turbomachinery as reported in [8], in the ranges between 0.1 to 1%. The higher end of this range corresponds to fundamental modes while the lower end is typical of higher order modes

3) SOLVER IMPLEMENTATION

The fluid-flow problem is characterized by the complete compressible Navier-Stokes equations. The corresponding mass, momentum and energy conservation equations are solved using the finite volume approach which are conservative as cell-based averaging of the edge fluxes. The solver is formulated to handle numerical error from non-orthogonality of the grid. In modelling the full-compressible flow equations, the discretization of the diffusion term was through a vertex-centered discretization scheme.

For the gradient term discretization, the scheme implemented computes the viscous gradient across each cell volume following the Green-Gauss solution approach. This is equivalent to computing the volume weighted cell average gradient, Correa et al. [10]. A second-order accurate scheme was used to compute the viscous term, with the stator and rotor meshes aligned in the flow direction, see Figure 3. The discretization method used for the convection term was the high-resolution scheme. This is also second-order accurate as compared to an ordinary upwind scheme which is only first-order accurate and can often lead to numerical diffusion in the solutions, [11]. The high-resolution scheme is also unconditionally stable. The balancing of fluxes was addressed using a flux-limiter based on the Total Variational Diminishing (TVD) approach of [12]. The temporal discretization of the transient term was obtained through the second-order backward Euler method. This is an implicit scheme and as such, is not prone to the numerical instability of the explicit models that are highly time-step size dependent.

The closure to the Navier-Stokes flow governing equations was provided through the shear-stress transport turbulence of Menter [13] . This model was modified with a wall function correction term as described in [14]. The blade rotational force was also modelled where in the rotor frame, the velocity field vector was modified to include the relative velocity field and an entrainment component, $\vec{v} = \vec{w} + \vec{u}$. It also necessary to ensure that the flow continuity equations remain invariant as the entrainment component does not contribute to the mass balance. Following the derivation proposed by Hirsch [15], the momentum conservation expression takes into accounts two force terms: the Coriolis force ($\vec{f}_{cr} = -2(\vec{w} \times \vec{\Omega})$) and that of the centrifugal force component ($\vec{f}_{cf} = \Omega^2 \times \vec{R}$). Where $\vec{R}$ is the position vector that is perpendicular to the rotational axis and Ω is the angular speed of the rotor wheel. The rotation effect does not affect the internal forces within the fluid, as these are not influenced by solid body motions in relation to other systems. Its effect, therefore, is mainly on the shear stress term and the stress tensor terms which are modified to include a relative velocity component. Finally, there is an additional work term from the centrifugal forces, while that of the Coriolis term is negligible in the energy equation. The rotational effect results in the rothalpy term which is in the form of a stagnation enthalpy in the rotating frame.

In setting up the corresponding boundary condition, the total pressure value was specified at the flow domain inlet boundary, while the static pressure value was specified at the outlet boundary. In specifying the normal gradient pressure term to the surface, an upwind scheme was implemented to enforce a zero pressure gradient across the outlet area. The blade was specified as a wall condition with a zero normal wall velocity. The errors in the discretized set of equations were quantified using the residual solution balance. The solution convergence was obtained when the monitored variables drop below 1e-04 at successive timesteps.

A domain interface condition was maintained at the periodic boundaries, as well as at the stator-rotor interface boundary. This was modelled to allow the changes in the frame of reference between the two domains. This was obtained through the Generic Grid Interface (GGI) mesh connection method, which allows for differing areas on both sides with mutually overlapping boundaries. Given that the stator-rotor interface does not match up exactly due to the pitch angle changes, a multiple frame of reference (transient rotor-stator) interface boundary was implemented to account for the time-averaged interaction effects. This provides a circumferential averaging of the fluxes at the domain interface.

In the current work, a single-passage analysis is performed in order to reduce the computational resources as required for a full wheel analysis. The formulation of a single passage analysis assumes that the test configuration exhibits cyclic symmetry with N identical replicas that close up to form a wheel with a phase-shifted periodic boundary condition. This enables a reference sector defined by a sector angle of $\beta = {}^{2\pi}/_{N}$ to be modelled [16]. As noted by Su et al. [17], this assumption allows for the simplification of the computation domain of the unsteady aerodynamic of the annular cascade to a single blade passage. These assumptions, however, are likely to be

violated in models having significant amount of mistuning between the component blades of the turbine wheel [18].

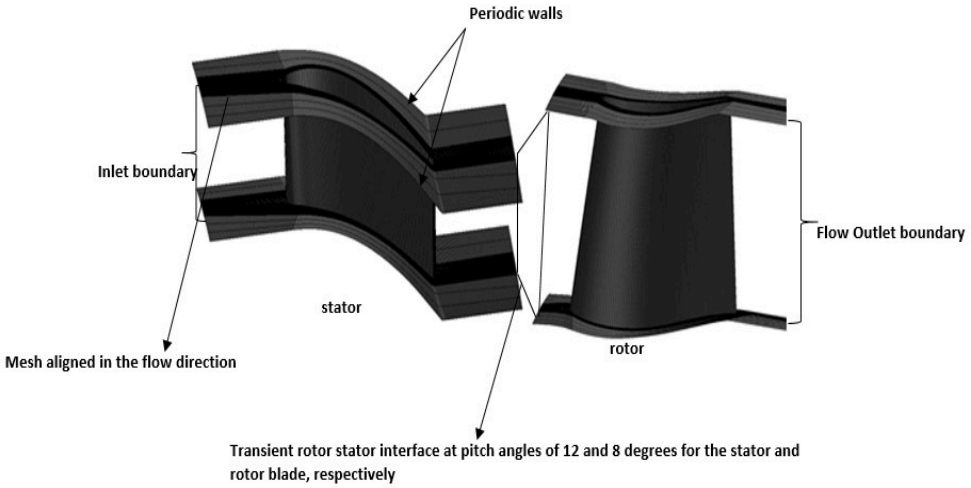

Figure 3 STATOR AND ROTOR BLADES MESH AND BOUNDARY PROFILES

On the solid-side finite element model, the problem was formulated following a forced response procedure with the bounding equation of motion of the form:

$$[M]\{\ddot{x}\} + [C]\{\dot{x}\} + [k]\{x\} = [F_A] + [F_R] \qquad 9$$

This represents a system of differential equation of second-order with an applicable standard solution procedure of either the direct integration or the mode superposition techniques as described in [19]. In equation 9, the terms $[M]$, $[k]$ are the mass and stiffness matrices for a blade nodal number, n, of a certain model eigenvector, $\{\phi_i, n\}$. The reaction forces on the right-hand side are: F_R which represents the forcing vector to account for the coriolis effect due to the high rotational speed and F_A is that due to the unsteady aerodynamic forces from the upstream stator wakes. Due to the effect of rotation, the overall system stiffness matrix is in the form, $[K] = [k_{el}] + [k_r] + [k_l] + [k_g]$. This accounts for the influence of the elastic, rotational, pre-strain and geometric stiffness terms, respectively. Also, the damping matrix $[C] = [c_{st}] + [c_r] + [c_{aero}]$; includes the effect of structural, damping and coriolis effect, and the aerodynamic damping effects. The structural damping terms are inherently estimated from the specified material conditions and rotational speed. The aerodynamic damping term was estimated from the monitored unsteady pressure signals on the rotor blade.

The test case analyzed in this study is the Vane-Blade Interaction (VBI) profile with experimental data obtained from Rao et al. [20]. This is a stator-rotor configuration formulated to investigate the unsteady aerodynamics and heat transfer characteristics of a turbine stage. The operating conditions for the stage are given in Table 1. The model is a transonic flow case with oblique shock-waves predicted at the stator blade row passage. Figure 3 also shows the 3D mesh profile of the stator and rotor blades.

From the solid-side equations, the equations of the partial differential equations of elasticity of the blade structure were solved using an energy approach from the virtual work formulations. The method is suitable for the small displacement bodies such as a turbine blade under an HCF condition, where the strain-displacement relations are maintained linearly [21], [22]. The blades' local displacements and load boundaries were modelled at distributed nodal points as the solutions are obtained using the isometric mesh-based shape functions.

Table 1 VANE-BLADE INTERACTION TEST CASE PARAMETERS

Parameters	Value
Inlet total pressure	303kPa
Inlet temperature	550K
Outlet Mach number	1.5
Number of stator blades	30
Number of rotor blades	45
Stator chord length (mm)	47.5
Rotor chord length (mm)	67.6
Rotational speed (rpm)	11450

4) SPECTRAL FATIGUE METHOD

The required parameters for fatigue estimation in the frequency domain can be directly obtained from outputs of the analysis formulated in the frequency domain or the transformation of the time-domain data using the Fourier transformation approach. In the frequency domain case, the model response is obtained by formulating the equation of motion through a modal decomposition procedure. Following the method presented in the Bracessi et al. [23], the physical displacement of the system can be obtained from the knowledge of the modal coordinates (or Langrangian coordinates) and the response frequency transformational matrix. Thus, the relationship between the frequency response in the Langrangian coordinate and the matrix of complex function can be directly obtained. This matrix of complex function is given in the form:

$$\mathcal{H}_q(\omega) = \mathcal{H}_n(\omega).A \tag{10}$$

Where $\mathcal{H}_n(\omega)$ is the transfer function matrix and A, in the case of a forced excitation, represents the transpose of the stress constraint modal transformation matrix in the frequency domain. For a simulation performed in the time domain, the stress signal data can be transformed into the frequency domain using the Fourier transformation approach. In this case, the Fourier transform of the stress tensor is made of two components: (1) product of the stress constraint modes matrix and Fourier transform of the constraints displacement and (2) the product of the stress mode shape and Fourier transform of the modal coordinate matrix. From the obtained stresses, the multiaxial nature of the loading can be described based on the six independent stresses, which can be represented in the vector; $\sigma_{(t)} = \left[\sigma_x, \sigma_y, \sigma_z, \tau_{xy}, \tau_{yz}, \sigma_{xz}\right]$. This six-dimensional random vector can be represented in the frequency domain using the six-dimensional random vector of the signal in terms of the two-sided power spectral density matrix:

$$P_\omega = \begin{bmatrix} \sigma_{11} & \cdots & \sigma_{16} \\ \vdots & \ddots & \vdots \\ \sigma_{61} & \cdots & \sigma_{66} \end{bmatrix} \tag{11}$$

The diagonal elements represent the auto-spectral density function of the stress components, while the off-diagonal elements are the cross-spectral density function which are complex functions at instances $\boldsymbol{i \neq j}$. From the estimated six components of the normal and shear stress obtained from the time domain, the equivalent frequency domain stress PSD can be obtained from the correlation;

$$G_{eq}(\omega) = a(P)_\omega a^T \tag{12}$$

Where $\boldsymbol{a}$ is the matrix of directional cosine obtained from projection of the critical stress plane. This is also defined in the form of the three Euler angles considering a rotated coordinate system. In that case, matrix $\boldsymbol{a}$ represents the rotation matrix which links the critical plane to the averaged principal stress direction, [24]. With the understanding that fatigue damage is most probable on the most damaging plane, and from the knowledge of the stress covariance matrix, the maximum variance on the multiaxial plane can be obtained [25]. By using the criterion of the maximum normal and shear stress on the critical plane, the corresponding equivalent stress can be obtained. This enables the reduction of the complex multiaxial stress state to an equivalent uniaxial stress, which can be represented in the form;

$$\sigma_{eqv}(t) = \sigma(t)a^T = \sum_{i}^{6} a_i \sigma_i(t) \tag{13}$$

Where $\sigma(t)$ is the vector of suitable components of stress and a^T is the transpose of the vector of suitable coefficients as shown in Table 2

Given the high-amplitude unsteadiness of the turbine pressure fields, the stress history is often irregular and with significant mean stress components. To account for the mean stress effect, a method earlier proposed by Nieslony and Bohm [26] is implemented. This allows the transformation of the stress amplitudes prior to the determination of the equivalent stress state. The method can also be extended to operate directly on the PSD of the stress signal prior to the estimation of the spectral moments.

From the modification of the load history from the global mean value, the transformation was proposed in the form;

Table 2 EQUIVALENT STRESS PARAMETRS FROM THE CRITICAL PLANE APPROACH

a_i	σ_{max} and τ
a_1	$\frac{l_1^2 - l_3^2 + K(l_1 + l_3)^2}{1 + K}$
a_2	$\frac{m_1^2 - m_3^2 + K(m_1 + m_3)^2}{1 + K}$
a_3	$\frac{n_1^2 - n_3^2 + K(n_1 + n_3)^2}{1 + K}$
a_4	$\frac{2[l_1 m_1 - l_3 m_3 + K(l_1 + l_3)(m_1 + m_3)]}{1 + K}$
a_5	$\frac{2[l_1 m_1 - l_3 n_3 + K(l_1 + l_3)(n + n_3)]}{1 + K}$
a_6	$\frac{2[m_1 n_1 - m_3 n_3 + K(m_1 + m_3)(n_1 + n_3)]}{1 + K}$

$$\sigma_t(t) = [\sigma(t) - \sigma_m].K_{\sigma_m} \quad 14$$

The mean stress coefficient, K_{σ_m} was established following the Morrow's relation

$$K_{\sigma_m} = \frac{1}{1 - \left(\frac{\sigma_m}{\sigma_f'}\right)} \quad 15$$

Where σ_f' is the fatigue strength coefficient equal to 1200MPa for the steel alloy material. This value was obtained by fitting a power function to the material test data for the elastic and plastic strain life equations. The material data are those of a strain-controlled fatigue test. The curve fitting was obtained through a numerical optimization technique in MATLAB using the "**lsqnonlin**" function. A detailed description of this process can be found in Hyde et al. [27]. The corresponding material properties were reported in the ASM Handbook [28].

In relation to the modification of the PSD signal to account for the effect of mean stress, the proposed relation is of the form [26]:

$$G_T(f) = K(\sigma_m)^2 G_\sigma(f) \quad 16$$

Where $G_\sigma(f)$ is the PSD of the centered-signal is $[\sigma - \sigma_m]$ and σ_m is the mean stress in the signal and σ is the stress amplitude.

In order to assess the degree of rotation of the principal stress during the damage process, the Euler angle estimation is based on an averaging procedure using the weight function method of [29] [30]. The principal stress direction matrix is given by:

$$A = \begin{bmatrix} l_1 & l_2 & l_3 \\ m_1 & m_2 & m_3 \\ n_1 & n_2 & n_3 \end{bmatrix} \quad 17$$

Where l_i, m_i, n_i are the principal direction cosines. A direction cosine matrix is often employed for the transformation between Cartesian systems. Thus, under a time varying loading condition, the averaging of the nine components of the matrix violates the orthonormality condition during transformation. Another related difficulty is in the choice of the three independent elements out of the nine to be averaged, Carpinteri et al. [29]. The corresponding matrix of direction cosines can be expressed in terms of the Euler parameters: ϕ, θ, ψ as in [31]. These Euler angles therefore represent the three counter-clockwise rotations of the principal stress directional cosines. The mean directions of the principal stress axes are obtained via an averaging of the Euler angles, following the method earlier proposed by Carpinteri et al. [29] which is based on the use of suitable weight functions that are selected from the predominant factors influencing fatigue.

4.1 Spectral fatigue damage models

One of the most widely used empirical formulas for the estimation of the rainflow amplitude density is the Dirlik method, under a broad-band loading spectrum. It is a sum of the Rayleigh probability density and the exponential cycle distributions. The Dirlik's damage probability density is given by;

$$f_\sigma(\Delta\sigma) = \frac{1}{\sigma_x}\left[\frac{D_1}{Q}e^{-\frac{Z}{Q}} + \frac{D_2 Z}{R^2}e^{-\frac{Z^2}{2R^2}} + D_3 Z e^{-\frac{Z^2}{2}}\right] \quad 18$$

Where the corresponding terms are defined as:

$$R = \frac{\gamma - \lambda_\xi - D_1^2}{1 - \gamma - D_1 - D_1^2} \quad 19$$

$$Z = \frac{\sigma_a}{\lambda_0} D_1 = \frac{2(\lambda_\xi - \gamma^2)}{1+\gamma^2}, \quad \lambda_\xi = \frac{\lambda_1}{\lambda_0}\left(\frac{\lambda_2}{\lambda_4}\right)^{0.5},\ D_2 = \frac{1-\gamma-D_1+D_1^2}{1-R}, D_3 = 1 - D_2 - D_3, \quad D_4 = \frac{1.25(\gamma - D_3 - D_2 R)}{D_1} \quad 20$$

While numerous studies have highlighted the accuracy of the above equations, it is worth mentioning that the method in its current form does not account for mean value dependence. It proposes the estimation of the probability densities as only dependent on the stress amplitude value. From the obtained stress projection, the method enables the damage per unit time to be estimated for a wide-band process. Given this current limitation, a recently formulated model in the frequency domain is that proposed by Tovo-Benasciutti [32], where the power spectral density function of the equivalent stress is obtained via the sums of suitable weight functions. This was proposed for the determination of the expected damage rate due to the amplitude of the rainflow counted cycles. The damage from the rainflow counting method was represented as a weighted sum in the form:

$$D_{RFC} = b_{app} D_{NB} + \left(1 - b_{pp}\right) D_{RC} \quad 21$$

Correspondingly, the probability density function for the rainflow counted amplitudes is given as:

$$f_\sigma(\Delta\sigma) = b_{app}\gamma\frac{\sigma_a}{\lambda_0} exp\left(\frac{-\sigma_a^2}{2\lambda_0}\right) + \left(1 - b_{app}\right)\frac{\sigma_a}{\gamma^2\lambda_0} exp\left(\frac{-\sigma_a^2}{2\gamma^2\lambda_0}\right) \quad 22$$

The weighting coefficient, b_{app} is given by;

$$b_{app} = \frac{(\alpha_1 - \alpha_2)\left[1.112\left(1 + \alpha_1\alpha_2 - (\alpha_1 + \alpha_2)\right) exp^{2.11\lambda_2} + (\alpha_1 - \alpha_2)\right]}{(\alpha_1 - 1)^2} \quad 23$$

And the spectral parameter α_m is defined by:

$$\alpha_m = \frac{\lambda_m}{\sqrt{\lambda_0\lambda_m}} \quad 24$$

In comparison to the rainflow damage estimation, each stress peak is paired with a lower range which results in the estimated expected rate of loading being equal to the expected rate of peaks. The narrow-band fatigue damage component, D_{NB}, in equation 21 is obtained via the Wirsching and Light [33] correlation given in the form;

$$E[D_{RFC}^{WL}] = \chi . E[D_{NB}] \quad 25$$

And

$$\chi = (0.926 - 0.033k) + [1 - (0.926 - 0.0033k)]\left(1 - \sqrt{1 - \alpha_2^2}\right)^{1.587k - 2.323} \quad 26$$

The damage in the narrow-band range can be estimated using:

$$E[D_{NB}] = v_p C^{-1}\left(\sqrt{2\lambda_0}\right)^k \Gamma\left(1 + \frac{k}{2}\right) \quad 27$$

$$D_{RC} = v_p C^{-1}\left(\sqrt{2\lambda_0}\alpha_2\right)^k \Gamma\left(1+\frac{k}{2}\right) \quad 28$$

The above correlations for the determination of the expected damage is dependent on three spectral parameters; $\lambda_0, \lambda_2, \lambda_4$, representing the zeroth-order, second-order and fourth-order spectral moments, respectively. The term Γ is the gamma function while α_m is the spectrum width parameter and k and c are obtained from the material S-N curve ($s^k N = c$), where k is the S-N curve slope, while c is the intercept. This can also be obtained using the Basquin correlation ($N = \left({}^{\sigma_a}/_{\alpha}\right)^{1/\beta}$), where $\beta = -1/k$ and $\alpha = 0.5c^{-\beta}$ and $\sigma_a = 0.5\Delta\sigma$. Thus, from the assumption of linear damage summation based on the Palmgren-Miner approach, the fatigue damage can be estimated from the integral:

$$D = \frac{T.n}{C}\int_0^{\infty} (\Delta\sigma)^k f_\sigma(\Delta\sigma) d(\Delta\sigma) \quad 29$$

Where $f_\sigma(\Delta\sigma)$ is the probability density function of the stress range cycles and n is the cycle count for each stress range from rainflow counting process.

Also, in order to account for any non-Gaussian nature of the load stress, Palmieri et al. [34] proposed the relation;

$$\lambda_{ng} = exp\left(\frac{m^{2/3}}{\pi}\left(\frac{k-3}{\pi} - \frac{S^2}{4}\right)\right) \quad 30$$

$$D_{ng} = \lambda_{ng} * D_g \quad 31$$

In this case, where k is the kurtosis and S is the skewness. m is the slope of the S-N curve

5) RESULTS

5.1 Unsteady flow case

Figure 4and Figure 5 show the coefficient of pressure estimation for the stator and rotor blades, respectively. In both cases, the flow unsteadiness on the suction surface is highly noticeable with separation and re-attachment at approximately 60-90% chord positions. In the model set-up, the inflow velocity and pressure were specified as normal to the inlet plane with the stagnation flow properties in the non-rotating frame set to standard temperature and pressure values. The high-rotational speed of the rotor blade at 11,450 rpm created a strong axial and whirl velocity components through the passage with a resulting increase in the flow Mach number across the stage. This led to strong pulses of flow seperation and re-attachment on the suction side of the rotor blade. A similar degree of unsteadiness was also noticed on the rotor suction surface

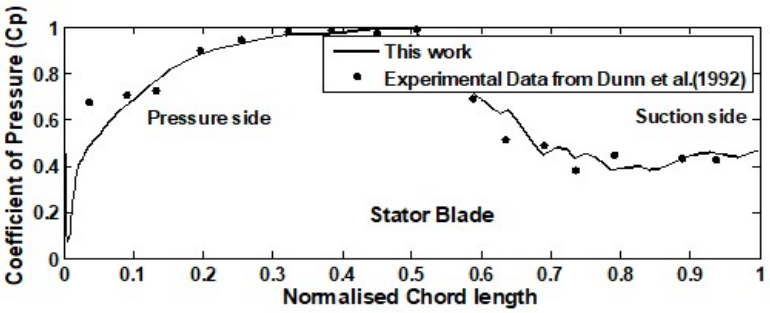

Figure 4 COEFFICIENT OF PRESSURE PREDICTION FOR STATOR BLADE

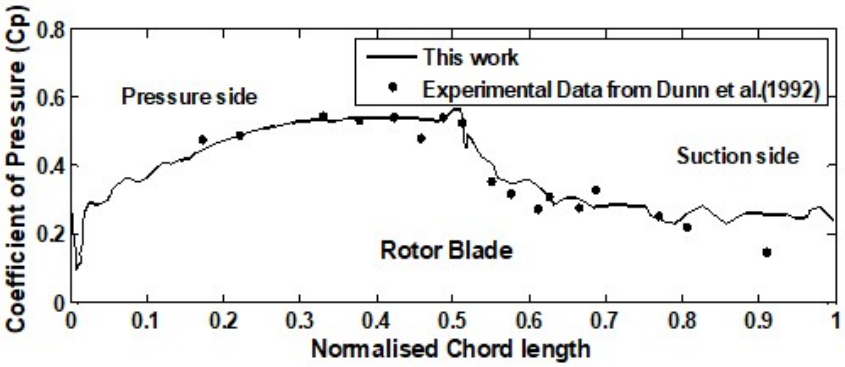

Figure 5 COEFFICICNET OF PRESSURE PREDICTION FOR ROTOR BLADE

The plots show the ensemble-averaged quantity of the coefficient of pressure plot in comparison with the experimental data which were also computed for the validation of the fluid-side solver, CFX. In both cases of the stator and rotor blades, the code predicted the pressure distribution closely matching the experimental data on the pressure surface, in the regions indicated by normalized chord length 0-0.5. In the suction surfaces prediction, the mean-value summation also predicts the unsteadiness very closely for the rotor blade, while a slight disparity is noticeable at the 0.9 location of the normalized chord length on the suction surface of the stator blade. In this case, the CFX-solver over predicts the static pressure by almost 30%. The unsteadiness in the suction surface side is mainly due to the unsteady shock-waves that perturbs the boundary-layer with a stronger influence noticeable on the rotor-blade case. Despite this unsteadiness, the fluid-flow code is demonstrated to be able to predict such complex flow phenomena with reasonable accuracy in comparison to the experimental data. The subsequent analyses will highlight the fatigue response noting the influence of the unsteady aerodynamic fields

5.2 Results – fatigue analyses

The predicted first four natural frequencies of the blade were 4408Hz, 6104Hz, 10248Hz and 11225Hz, respectively. At the operational speed range, the first excitation and resonance condition from the unsteady pressure field was noticed at the 23rd-Engine order (EO), where the frequency is 4389Hz and is 18Hz less than the blade's first bending mode. Similarly, for the second torsional mode with frequency of 6104Hz, the closest engine-order frequency was 6106Hz which is for the 32nd EO. With approximately 30 upstream stator blades, both cases show the blade in a detuned condition to avoid possible resonances in the first two modes. It was also the case that, at the higher-order third and fourth natural frequencies, the excitation sources were also outside the operational range of the engine.

The corresponding equivalent stress and displacement contour plots were qualitatively similar for both simulation approaches as shown in Figure 6. The stress history PSD from the uncoupled and fully-coupled simulation cases is shown in Figure 7**.** These were obtained from the earlier presented methods for equivalent stress determination in the frequency domain, [35] [36] [31] based on the normal and shear stress components. The matrix of the equivalent stress was then formulated as a cross-spectral density matrix with the correlation and auto-correlation terms in the off-diagonal and diagonal components, respectively. The model of the multiaxial fatigue criterion using the PSD of the equivalent stress were computed from Fourier transformation approach. Having established the equivalent stress state, the fatigue life can be evaluated based on the theory of linear damage summation. Thus, from the critical plane assumption, the material fatigue strength under a uniaxial random loading is dependent on the stress amplitude, the critical plane parameter and the material fatigue properties. This allows the surface of the limit state of the fatigue life to be determined based on the limit value of the fatigue strength function. Thus, the use of the critical plane for the equivalent stress reduction is therefore useful in avoiding the pitfall of the classical von Mises approach which is not able to account for the effect of hydrostatic stresses in the fatigue life.

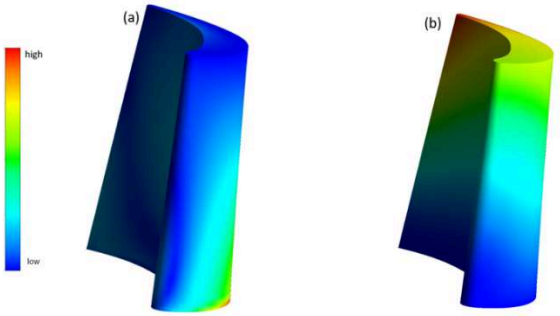

Figure 6 CONTOUR PLOTS OF von MISES STRESS AND DISPLACEMENT

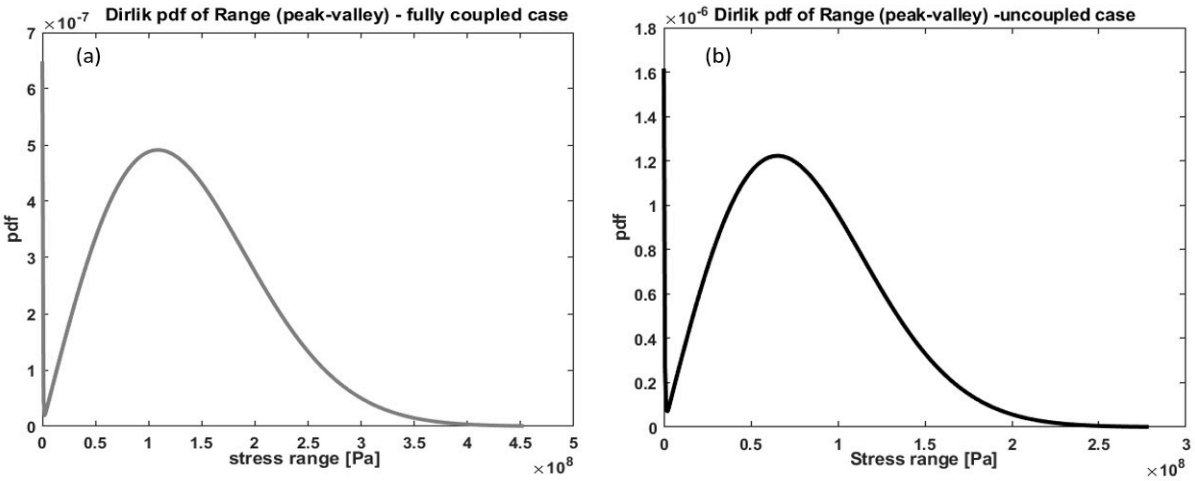

Figure 7 DIRLIK PDF OF (a) FULLY-COUPLED AND (b) UNCOUPLED APPROACHES

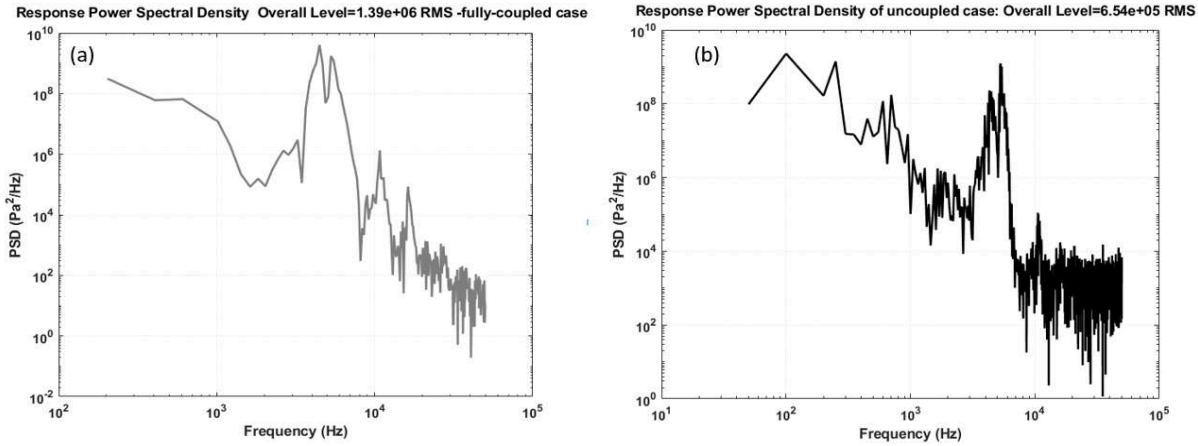

Figure 8 POWER SPECTRAL DENSITY OF (a) FULLY-COUPLED AND (b) UNCOUPLED APPROACHES

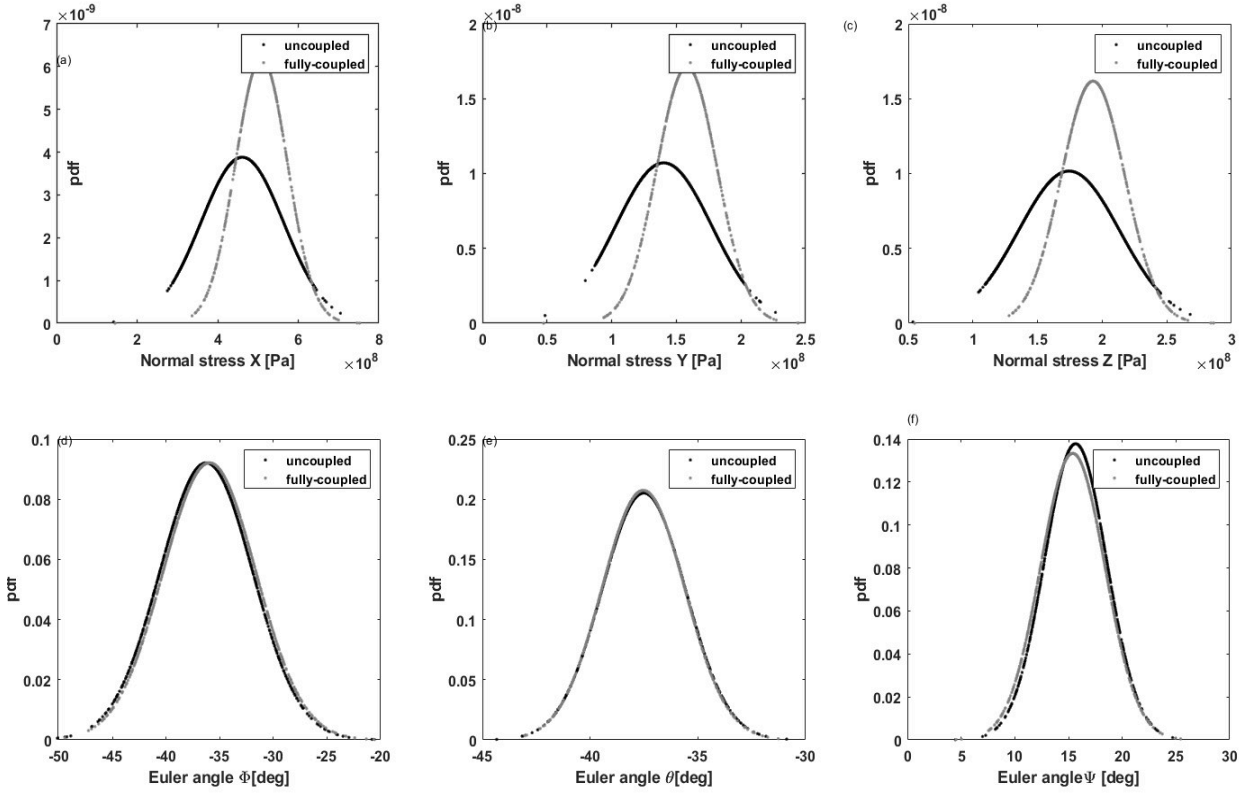

Figure 9 PDF OF (a) NORMAL STRESS X (b) NORMAL STRESS Y (c) NORMAL STRESS Z (d) EULER ANGLE 1 (e) EULER ANGLE 2 (3) EULER ANGLE 3

Table 3 FATIGUE DAMAGE ESTIMATION FOR THE UNCOUPLED METHOD

Stress [Pa]	PDF	D_{Dirlik}	D_{TB}	n	N	D_{RFC}	EI_{Dirlik}	EI_{TB}
8.45E+07	1.13E-06	8.55e-04	8.47e-04	76	435299	1.75e-04	0.69	0.68
9.71E+07	9.94E-07	1.19E-03	1.17E-03	90	212638	4.22E-04	0.45	0.44
1.12E+08	8.00E-07	1.46E-03	1.44E-03	103	101873	1.01E-3	0.16	0.15
1.26E+08	6.10E-07	1.58E-03	1.56E-03	114	55512	2.05E-03	0.11	0.12
1.38E+08	4.63E-07	1.63E-03	1.60E-03	120	34732	3.45E-03	0.33	0.33
1.63E+08	2.22E-07	1.65E-03	1.62E-03	127	14723	8.63E-03	0.72	0.73
1.80E+08	1.25E-07	1.65E-03	1.63E-03	130	8829	1.47E-02	0.95	0.96
2.03E+08	5.50E-08	1.65E-03	1.62E-03	132	4750	2.78E-02	1.23	1.23
2.17E+08	2.69E-08	1.65E-03	1.62E-03	132	3368	3.92E-02	1.37	1.38

Table 4 FATIGUE DAMAGE FOR THE FULLY-COUPLED METHOD

Stress [Pa]	PDF	D_{Dirlik}	D_{TB}	n	N	D_{RFC}	EI_{Dirlik}	EI_{TB}
8.17E07	4.59E-7	1.14E-03	1.14E-03	23	517873	4.39E-05	1.41	1.41
1.11E8	4.91E-07	5.09E-03	5.09E-03	33	106693	3.11E-04	1.21	1.21
1.41E08	4.54E-07	1.18E-02	1.18E-02	52	31088	1.66E-03	0.86	0.85
1.61E08	4.0E-07	1.61E-02	1.61E-02	59	15691	3.78E-03	0.63	0.63
1.79E08	3.43E-07	1.90E-02	1.90E-02	66	9086	7.32E-03	0.42	0.42
2.06E08	2.57E-07	2.17E-02	2.14E-02	75	4404	1.69E-02	0.11	0.10
2.24E08	2.01E-07	2.24E-02	2.21E-02	79	2860	2.76E-02	0.09	0.10

Figure 8 shows the estimated PDF for the uncoupled and fully-coupled solution methods. This is obtained using the Dirlik rainflow counting approach which is based on the peak-valley stress amplitudes. As shown, the estimated PDF of the uncoupled is higher than that of the fully-coupled case by an order of magnitude. The differences in the two approaches are also illustrated in Figure 9, where the distributions for the three directional normal stresses are shown, as well as the Euler angles indicating the rotation of the stress principal directional stresses.

The method of multiaxial critical plane method implemented is that of the maximum shear and normal shear , which also takes into account the weighted-average summation of the directional cosines of the three principal stresses arranged in decreasing order: $\sigma_1 \geq \sigma_2 \geq \sigma_3$. Thus, at the material final failure phase, the plane of fracture is often that of the maximum shear planes for a ductile material. While for semi ductile and brittle materials, the fracture plane can fluctuate between that of the normal stress and that of the maximum strain energy density [29]. In both cases of the fully-coupled and uncoupled stress histories, the ratios of the shear stress amplitude to the normal stress value were less than 0.63 (0.08 for the un-coupled and 0.08 for the fully-coupled case), depicting that the final fracture plane is predominantly influenced by the plane on which the normal stress and the strain energy density obtain their maximum. For metallic materials, the planes of intensified slip, i.e. the crystallographic planes, are also the planes of maximum shear as these are often sites for crack initiation. Thus, by considering a typical mode I crack growth case, the slip process and decohesion in front of the crack are mainly shear plane driven. A similar understanding can be applied to the stage II propagation phase, where the maximum shear strain controls the slip and decohesion process, while the dislocation mobility can be controlled by the tensile strain parameter, [37].

From the predicted PSD of Figure 8, the root-mean-square of the signal from the fully-coupled case is higher than that of the uncoupled method, which also depicts a higher magnitude and strength of the signal. Based on the Dirlik rainflow counting approach, the cycle histograms of the two stress signals were also estimated. The relevant spectral moments for the uncoupled case were: 1.07e+15, 4.6936e+18, 2.0617e+22 and 4.0138e+29, representing the zeroth, first, second and fourth spectral moments. The corresponding case for the fully-coupled solutions were: 2.968e+15, 1.3038e+19, 5.7443e+22 and 1.1216e+30. Despite the high-magnitude of the spectral moments which tend to depict a wide-band process, the PSD shows both cases to be nearly bimodal with only two significant frequency contents. The wide band nature can result from the smaller signal strengths having high frequency values but do not necessarily contribute to the fatigue damage due to their low signal strengths. Based on the equivalent stress obtained in the critical plane approach, the fatigue lives were calculated using the Dirlik and Tovo-Benasciutti (TB) correlations presented earlier. The estimated fatigue life from both simulation methods are shown in Table 3 and Table 4

6) DISCUSSION

The PSD estimation for both cases show the responses to be predominantly bimodal, with lower frequency values at 4400Hz and 6150Hz for the fully-coupled process and 4400Hz and 6200Hz for the uncoupled case. These two response frequencies closely match the blades first two natural frequency at 4408 Hz and 6104 Hz, respectively for the bending and torsion modes. A higher mean stress value was also noticed for the fully-coupled resulting in an increased signal power at one order of magnitude higher than that of the uncoupled process. As such, the average frequency of the process, describing the rate of up-crossings of mean values for both processes were also similar. The fully-coupled simulation method was estimated as 4389 Hz, while 4400Hz was estimated for the uncoupled process. Similarly, the spectral width parameter, α_2 which is the irregularity factor, was also coincident for both simulations at 0.995 and 0.996, respectively for the fully-coupled and uncoupled processes. This indicates that both processes can be described as narrow-band signals. In analyzing the fatigue life, some of the smaller multimodal secondary peaks are included with truncation applied to the low PSD values, lower than the first natural mode. The spectral method is therefore, able to deal with such variations in a gradually decaying PSD [38]. The truncation of the significantly low-frequency content and the significantly low spectral density regions were mainly from the observable rainflow cycle count. The cumulative cycles tended towards an asymptotic value at the higher stress cycle ranges. This meant that the value of the estimated fatigue damage did not reduce beyond 20% at these higher frequency ranges. A similar rule of thumb was adopted in [38] for truncating higher and lower frequency ranges.

From the damage accumulation estimation using the Tovo-Benasciutti (TB) method, the narrow-band damage component was predicted using the Wirsching and light equation. This considers the rate of cycle occurrence as the occurrence of the positive peaks in the process. Each range is twice that of the positive peak which enables the rate of occurrence to be estimated based on the two spectral moments, λ_2 and λ_4. Thus, the probability distribution is then determined with an additional spectral component, λ_0. Despite the similarity in the spectral width of the two processes, the cumulative damage predictions are markedly different for both the Dirlik and TB methods. The ability of the TB method to predict the fatigue life using four spectral moments offers a higher accuracy than methods such as the Rayleigh approach which only depends on a single spectral moment. The time-domain fatigue damage using the rainflow cycle count approach is also shown in Table 3 and Table 4. The predicted stress histories were analyzed using a rainflow algorithm, which simulates the peaks and valleys for each identified stress range. The adopted rainflow analysis code was developed by Irvine [39], which also included an empirical method for cycle identification. From the data shown in Table 3 and Table 4, it is estimated that the maximum error from the TB and Dirlik methods, in relation to the time domain analyses, seems to be increasing with increasing stress amplitude. These differences are highlighted using the Error Index (EI) factor. As shown, both methods of spectral damage estimation predicted the same level of accuracy in relation to the time-domain linear damage summation approach for the fully-coupled stress history. However, the corresponding time-domain damage in the uncoupled method was higher as compared to the predictions obtained using the frequency domain methods.

Also, by using the Dirlik and TB methods which are derived based on the assumption of a Gaussian and stationary load case, it is evident from the predicted load histories of both simulation approaches that these conditions of "Gaussianity" and stationarity of the response history are violated. This is evident by the closeness of the vibrating frequencies to the natural frequencies of the blade. It is generally the case that such closeness of the response frequency to the component's natural frequency tend to portray a non-normality assumption [34]. This was also by verified by considering such spectral parameters as the skewness, s, kurtosis k and the crest factor, ς. The kurtosis describes the sharpness of the peak and width of the tail of the PDF. It is an indication of the concentration of the samples around the mean value. Skewness on the other hand, defines the degree of asymmetry of a data for a non-Gaussian case. The skewness measures the asymmetry of the PDF. A characteristic Gaussian distribution can be defined by $s = 0$ and k= 3. Thus, for a distribution with $k > 3$, it entails a sharper peak and wider tails of a non-Gaussian nature. Similarly, for kurtosis, k, values greater than 3, the process can be described as leptokurtic, whereby the fatigue damage estimated are higher than those of a typical Gaussian type. The stress history for the fully-coupled and uncoupled solution approaches have a kurtosis value of 2.3 and 2.9, respectively. The skewness values for the two solution methods were -0.2 and 0.19 for the uncoupled and fully-coupled processes, respectively. While a positive skewness indicates that the tail of the distribution is to the right, a negative value indicates a longer tail to the left-side of the distribution. It is also the case that, for kurtosis values less than 3, the process can be described as platykurtic with less probability mass near its mean value and in the tail region of the distribution, in comparison to a Gaussian process with equal standard deviation.

In determining whether a distribution is Gaussian or non-Gaussian, the influence of kurtosis is more considerable than that of skewness, [34] [40]. Generally, if the non-Gaussian history is stationary, the application of classical frequency-counting approach predicts fatigue lives that are comparable to those from Gaussian

considerations. However, inaccurate results may be obtained for such assumptions on a non-stationary non-Gaussian loading. As shown in both values of kurtoses predicted above, the two distributions can be described as stationary but cannot be fully regarded as Gaussian. In correcting for this non Gaussian effect, the fatigue damage obtained from the Gaussian-based assumption was then multiplied by the corrective coefficient, λ_{ng} of equation 30. In the uncoupled process, $\lambda_{ng} = 0.536$ while in the fully-coupled process, $\lambda_{ng} = 0.857$. At $\lambda_{ng} = 0.536$, this indicates that the predicted fatigue life would be 85% longer than that predicted assuming a Gaussian process. Similarly, at $\lambda_{ng} = 0.857$, the predicted fatigue life is 16% longer than a comparable prediction using the Gaussian method. This noticeable non-Gaussian effect can be attributed to the nonlinearity present in the model, which may arise in an instance where the induced stresses are closer to the material yield stress or those with significant plastic strains.

The differences in the stress histories of the two simulation approaches can also be seen in the disparity of the PDF distributions of the three principal stress states. This is shown in Figure 9. For the three directional normal stresses, the fully-coupled method shows a sharper peak with a rapidly dropping tail, as compared to the predictions from the uncoupled method. Also shown on this figure is the density distribution of the weighted average Euler angles depicting the orientation of the principal stresses to the model axes. As shown in the time-plot of the three principal Euler angles, the components are continuously varying with the time history, where a similar PDF distributions for both processes was obtained. The averaging procedure adopted for decomposing the angles were restricted to the range $-{}^{\pi}/_{2} \leq \psi, \theta, \phi \leq {}^{\pi}/_{2}$. This degree of orientation of the principal stress angles depicts a non-proportional loading behaviour which can easily induce more fatigue cracks as compared to a proportional loading case. This is the case when the rotation of the principal stress direction leads to the activation of the slip bands in the material grains, [41]. In the presence of high-mean stresses, the position of the critical plane would therefore be influenced, not only by the directions of the maximum principal stress and material constant, but also by the variable and static stress magnitudes [42]. Characteristically, for a turbine blade, these torsional and bending stresses easily arise due to the combined influence of the rotational and unsteady pressure forces. The corresponding mean stresses are high when compared to the variable stress amplitudes and therefore results in the position of the critical plane approaching the plane of the maximum principal stresses.

Finally, from the fatigue damage estimations of Table 3 and Table 4, it is shown that the Dirlik method and the Tovo-Benasciutti approaches predict the error index to within a similar band. This also shows their accuracy in the relation to the time-domain rainflow cycle method. While this is true for the low-stress ranges, the disparity between these two frequency domain methods increases as the nonlinearity in the stress-strain response increases, near yielding. In using these methods, it is important to note that for the Dirlik method, its derivation is not supported by any theoretical justification, and the estimation of the PDF is amplitude dependent, which may not allow for the model extension to accurately account for the mean stress effects. A similar argument is applicable to the time-domain method adopted here, which is the Palmgren-Miner time domain approach. In the Palmgren-Miner approach, the underlying assumption is that the stress history is considered as a stationary stochastic process. Thus, the fatigue damage grows linearly with time when the stress history behaves as a stationary and stochastic signal. This is often not true and can at times require the application of a correction method for damages estimated based on the narrowband assumption. The accuracy of the method is therefore dependent on the rainflow cycle counting method adopted, which varies depending on the mode of crack propagation considered [43]. Despite the above noted limitations, the study has demonstrated an approach for the application of spectral damage assessment methods for a turbine blade fatigue life evaluation at the high-cycle fatigue load range. The accuracy of the approach is comparable to the time domain Palmgren-Miner method at the lower stress ranges, where there is no significant impact of nonlinearity in the materials stress-strain response. Apparently, the fatigue damage in the fully-coupled stress history is conservative in relation to that from the uncoupled simulation approach.

7) CONCLUSION

Fluid-structure interaction studies were implemented for the investigation of vibration-induced fatigue response of a high-pressure turbine blade. Two coupling methods; a fully-coupled and an uncoupled solution approach were implemented. In the fully-coupled approach, the solutions of the fluid-flow and structural finite element code were obtained simultaneously per solution timestep. This ensures a tightly coupled case using a fluid-solid interface condition as an intermediary between the two domains. On the other hand, the uncoupled analysis involved a separate analysis of the unsteady flow field followed by the estimation of the structural modal response, with the estimated pressure field as the forcing function. The aerodynamic damping from the approach is obtained from a separate log-decrement analysis of the unsteady pressure field data.

The fatigue lives were analyzed in the frequency domain based on the two commonly adopted methods: the Dirlik method and the Tovo-Benasciutti method. While both methods are based on the Gaussian and stationary assumption, the loading responses from the fully-coupled and uncoupled stress histories violate these assumptions

as a result of the non-linearity present at the predicted higher stress ranges. Both spectral methods predict the fatigue life accurately in the lower stress range, in relation to the time-domain rainflow approach. The applicability of the method reduces significantly at higher stress ranges where, due to the closeness of the predicted stress range to the material yield strengths, there is a rapid acceleration of the fatigue damage in both the uncoupled and fully-coupled solution methods. Comparatively, the effects of the fluid-structure interaction from the two simulation approaches show the fully-coupled approach to be the conservative approach, in relation to the uncoupled solution method. Thus, while the adopted frequency domain approaches can be readily adopted for fatigue damage assessment in the lower stress ranges with little or no explicit plasticity present, further improvements are required before such methods can be applied to elastic-plastic failure related modes.

8) ACKNOWLEDGEMENT

The author wishes to thank Cranfield University Centre for Propulsion Engineering for providing the computing resources used to carry out this study

9) References

[1] M. Platzer and F. Carta, "AGARD Manual on Aeroslasticity in Axial-Flow Turbomachines," Volume 2 of ARD series on Structural Dynamics and Aeroelasticity, Essex, 1988.

[2] S. Fleeter, C. Zhou, E. N. Houstis and J. Rice, "fatigue Life prediction of Turbomachine Blading," nt of Computer Science technical Report 99-030, Purdue University, Indiana, 1999.

[3] G. Halford, T. G. Meyer, D. M. Nissley and G. A. Swanson, "Fatigue Life Prediction Modeling for Turbine n," NASA lewis REsearch Center, USA, 1989.

[4] A. Carpinteri, G. Fortese, C. Ronchei, D. Scorza and A. Spagnoli, "Fatigue Life Evaluation of Metallic under Multiaxial Random Loading," *International Journal of Fatigue,* pp. Vol.90, page 191-199, 2016.

[5] D. Benasciutti, F. Sherrat and A. Cristofori, "Basic principles of Spectral Multi-axial Fatigue Analysis," *Engineering,* vol. 101, pp. 34-42, 2015.

[6] R. Zwaan and B. B. Prananta, "Fluid/Structure Interaction in Numerical Aeroelastic Simulation," *nal Journal of Non-linear Mechanics,* vol. 37, pp. 987-1002, 2002.

[7] J. Leger, "Development of an Unsteady Aeroelastic Solver for the Analysis of Modern Turbomachine A PhD Thesis of Wright State University, USA, 2010.

[8] Y. El-Aini, R. deLaneuville, A. Stoner and V. Capace, "High-Cycle Fatigue Life of Turbomachinery nts - Industry Perspective," *AIAA Journal,* pp. 1-9, 1997.

[9] D. A. Gottfried and S. Fleeter, "Aerodynamic Damping Predictions for Turbomachinery Blade Rows using imension Time Marching Simulations," Purdue University Report 99-026, USA, 1999.

[10] C. D. Correa, R. Hero and K. L. Ma, "A Comparison of Gradient Estimation methods for Volume Rendering ctured Meshes," *IEEE Transactions on Visualization and Computer Graphics,* pp. 1-14, 2011.

[11] F. Moukalled, L. Magani and M. Darwish, The Finite Volume Method in Computational Fluid Dynamics: ced Introduction with OPENFOAM and MATLAB, Switzerland: Springer International, 2016.

[12] A. Harten, "High Resolution Schemes for Hyperbolic Conservation Laws," *Computational Physics,* vol. 49, 03, 1983.

[13] F. Menter, "Two-Equations Eddy-Viscosity Turbulence Modelss for ENgineering Applications," *AIAA* ol. 32, no. 8, pp. 269-289, 1994.

[14] F. Menter, "Review of the Shear-Stress Transport Turbulence Model Experience from an Industry e," *International Journal of Computational Fluid Dynamics,* vol. 23, no. 4, pp. 305-316, 2009.

[15] C. Hirsch, Numerical Computation of Internal and External Flows, Volume 1 Fundamentals of onal Fluid Dynamics, Oxford: John Wiley and Sons, 2007.

[16] D. M. Tran, "Multi-Parameter Aerodynamic Modeling for Aeroelastic Coupling in Turbomachinery," *f Fluids and Structures,* vol. 25, pp. 519-534, 2009.

[17] D. Su, W. Zhang and Z. Ye, "A Reduced Order Model for Uncoupled and Coupled Flutter Analysis," *Journal nd Structures,* vol. 61, pp. 410-430, 2016.

[18] E. Petrov, L. D. Mare, H. Hennings and R. Elliot, "Forced Response of Mistuned Bladed Disc in Gas Flow: ative Study of Predictions and Full-Scale Experimental Results," in *Proceedings of ASME Turbo Expo 2009; Land, Sea and Air, GT2009-59632*, Florida, USA, 2009.

[19] K. J. Bathe, Finite Element Procedures, New Jersey: Prentice Hall, 1996.

[20] K.V.Rao, R.A.Delaney and M.G.Dunn, "Vane-Blade Interaction in a Transonic Turbine , Part 1: nics," *Journal of Propulsion and Power,* vol. 10, no. 3, pp. 305-311 , 1994.

[21] Hirofumi Doi, "Fluid/Structure Coupled Aeroelastic Computations for Transonic flows in Turbomachine," University, USA, 2002.

[22] O. A Bachau and J. I. Craig, Structural Analysis (with Applications to Aerospace Structures), USA: Springer Business Media, 2009.

[23] F. Cianetti, M. Palmieri, C. Braccessi and G. Morettini, "Correction Formula Approach to Evaluate Fatigue nduced by non-Gaussian Stress State," *Procedia Structural Integrity,* vol. 8, pp. 390-398, 2018.

[24] A. Carpinteri, A. Spagnoli and S. Vantadori, "A Critical plane-based criterion for high-cycle multiaxial ing averaged principal stress directions," Dept. of Civil and Environmental Engineering, Parma, Italy,

[25] E. Macha and A. Nieslony, "Critical Plane Fatigue Life Models of Materials and Structures under Multiaxial Random Loadings: The State-of-the-art in Opole Research Centre CESTI and Directions of Future ," *International Journal of Fatigue,* vol. 39, pp. 95-102, 2012.

[26] A. Nieslony and M. Bohm, "Frequency-domain Fatigue Life Estimation with Mean Stress Correction," *nal Journal of Fatigue,* vol. 91, pp. 373-281, 2016.

[27] Y. P. Gong, C. J. Hyde, W. Sun and T. H. Hyde, "Determination of Material Properties In The Chaboche iscoplaticity Model," *Proc. IMechE Journal of Materials: Design and Applications,* vol. 224, no. 273, pp. 6.

[28] Bruce Boardman, Deere and Company,Technical Center, "Fatigue Resistance of Steel," *ASM Handbook: and Selection: Irons, steels and High Performance Alloys,* pp. ASM Handbook Committee, p 673-688,

[29] A. Carpinteri, A. Karolczuk, E. Macha and S. Vantadori, "Expected Position of the Fatigue Fracture Plane ne Weighted Mean Principal Euler Angles," *International Journal of Fracture,* vol. 115, pp. 87-99, 2002.

[30] A. Carpinteri, E. Macha, R. Brighenti and A. Spagnoli, "Expected Principal Stress Directions under Random Loading. Part I: Theoretical Aspects of the Weight Function Method," *International Journal of* ol. 21, pp. 83-88, 1999.

[31] Z. Marciniak and D. Rozumek, "Professor Ewald Macha's Contribution to the Development of Methods for Fatigue Life Estimation," *International Journal of Fatigue,* vol. 92, pp. 384-394, 2016.

[32] D. Benasciutti and R. Tovo, "Comparison of Spectral Methods for Fatigue Analysis of Broad-band Gaussian rocess," *probabilistic Engineering Mechanics,* pp. Vol, 21, page 287-299, 2006.

[33] P. Wirsching and C. Light, "Fatigue under wide band random stresses," *J. Struct Div ASCE,* vol. 106, pp. ', 1980.

[34] M. Palmieri, M. Cesnik, J. Slavic, F. Cianetti and M. Boltezar, "Non-Gaussian and Non-Stationarity in Fatigue," *International Journal of Fatigue,* vol. 97, pp. 9-19, 2017.

[35] Enrique de la Fuente, "von Mises Stresses in Random Vibration of Linear Structures," *Computers and* , pp. 1253-1262, 2009.

[36] A. Preumont and V. Piefort, "Predicting random high-cycle fatigue life with finite elements," *Journal of and Acoustics,* vol. 115, no. 2, pp. 245-248, 1994.

[37] M. W. Brown and K. J. Miller, "A theory for fatigue failure under multiaxial stress-strain conditions," *echanics group; Proc. Instn Mech Engrs,* vol. 187, no. 65, pp. 745-755, 1973.

[38] L. D. Lutes and C. E. Larsen , "An Improved Spectral Method for Variable Amplitude Fatigue Prediction," *Structural Engineering,* vol. 116, no. 4, pp. 1149-1164, 1990.

[39] T. Irvine, "Dirlik Rainflow Counting Method from Response PSD," Vibration Data, November 2013. Available: https://vibrationdata.wordpress.com/2013/11/08/dirlik-rainflow-counting-method-from-psd/.

[40] S. A. Rizzi, A. Przekop and T. Turner, "On the Response of a Nonlinear Structure to High Kurtosis Non-Random Loading," in *8th International Conference on Structural Dynamics - EURODYN2011*, Leuven, 2011.

[41] A. Karolczuk and E. Macha, "A Review of Critical Plane Orientations in Multiaxial Fatigue Failure Criteria c Materials," *International Journal of Fracture,* vol. 134, pp. 267-304, 2005.

[42] F. Stulen and H. N. Cummings, "A Failure Criterion for Multiaxial Fatigue Stresses," *Proc. ASTM,* vol. 54, 5, 1954.

[43] L. D. Lutes, M. Corazao, J. S.-l. Hu and J. Zimmerman, "Stochastic Fatigue Damage Accumulation," *Structural Engineering,* vol. 110, no. 11, pp. 2585-2601, 1984.

NOMENCLATURE

T_r	Trace operator
U^f	Fluid-solid interface variable
n	Unit normal vector
$d_f, \underline{d_s}$	Fluid and solid-side displacement
$\underline{\tau}$	Stress tensor
δ	Log-decrement damping
x_i, x_{i+1}	Peak and successive peak values of a signal
ζ	Damping decay constant
$\partial p/\partial n$	Pressure gradient
$[M]$	Mass matrix
$\{\ddot{x}\}$	Acceleration matrix
$[C]$	Damping matrix
$\{\dot{x}\}$	Velocity matrix
$[k]$	Stiffness matrix
$\{x\}$	Displacement matrix
$[F_A], [F_R]$	Aerodyanmic and rotational force vectors
$\mathcal{H}_q(\omega)$	Matrix of complex function
$\mathcal{H}_n(\omega)$	Transfer function matrix
A	Transpose of the stress constraint matrix
P_ω	Power Spectral density matrix
a	Rotational matrix
$G_{eq}(\omega)$	Equivalent power spectral density matrix
σ_i	Normal stress in direction i
$\sigma(t)$	Stress amplitude at time t
ϕ, θ, ψ	Euler angles for the 3-principal stresses
$f_\sigma(\Delta\sigma)$	Probability distribution
$E[D_{NB}]$	Expected damage from narrow-band process
D_{RC}	Damage from range counting
D	Time domain damage parameter
λ_{ng}	Non-Gaussian correction factor
t^i	Solution timestep at ith time
PSD	Power spectral Density

https://dspace.org/

Application of spectral method for vibration-induced high-cycle fatigue evaluation of an HP turbine blade

Ubulom, Iroizan

2020-11-11
American Society of Mechanical Engineers (ASME)
https://doi.org/10.1115/1.4049099
Ubulom I. (2021) Application of spectral method for vibration-induced high-cycle fatigue evaluation of an HP turbine blade. Journal of Engineering for Gas Turbines and Power, Volume 143, Issue 6, June 2021, Article number GTP-20-1395

Downloaded from a DSpace repository. https://dspace.org/